The architecture of the heart: A database model

Article *in* Philosophical Transactions of The Royal Society A Mathematical Physical and Engineering Sciences · June 2001

DOI: 10.1098/rsta.2001.0827

10.1098/rsta.2001.0827

THE ROYAL SOCIETY

The architecture of the heart: a data-based model

By Ian LeGrice[1], Peter Hunter[2], Alistair Young[1] and Bruce Smaill[1]

[1]*Department of Physiology, School of Medicine and*
[2]*Department of Engineering Science, School of Engineering, University of Auckland, Auckland, New Zealand*

An appropriate mathematical representation of heart structure is central to advancing an integrative approach to cardiac function. The Auckland heart model provides a realistic representation of important aspects of ventricular structure. The finite-element model is based on extensive anatomical data and incorporates detailed information on ventricular geometry and myocyte organization. It includes preliminary descriptions of the Purkinje fibre network, coronary vessels and collagen organization. Comprehensive extension of these data is required to exploit the full potential of computer modelling. In particular, we need to quantify the morphology of the atria, cardiac conduction system and the intramyocardial coronary vessels. This information must span an appropriate range of species and disease states.

Keywords: finite-element model; myocardial structure; fibrous laminar myocardium; geometry

1. Introduction

To obtain a more complete understanding of normal and abnormal cardiac function it is necessary to integrate a vast array of experimental information derived at cellular and subcellular levels. Computer modelling provides a powerful tool for advancing this integrative approach and appropriate mathematical representation of the anatomy of the heart is central to the process.

For example, experimental studies have provided comprehensive information about normal and pathological electrical function of ventricular myocytes. Despite this, the origins of re-entrant ventricular arrhythmia are poorly understood. Computer models appear to provide the most practical vehicle for investigating the genesis of many types of ventricular arrhythmia and exploring possible approaches to their treatment. It is generally accepted that the maintenance of ventricular arrhythmia may be influenced by the complex three-dimensional architecture of the ventricular myocardium as well as by spatial inhomogeneity of action potential characteristics. Any computer model used within this context should, therefore, incorporate important anatomical features within a framework that enables the inhomogeneous and anisotropic electrical properties of ventricular myocardium to be represented in an accurate and efficient manner.

Similar considerations apply to most of such integrative studies of cardiac function. Typically, we are dealing with boundary-value problems that require detailed

representations of relevant cardiac geometry. Because material properties are, in general, structure dependent it is necessary also to incorporate information relating to three-dimensional myocardial architecture. Anatomical models of the heart should be as compact as possible with structural information included at a scale and with an accuracy appropriate to the problem addressed. Finally, such models should be formulated in a way which enables efficient solution of the problem concerned.

Information available on cardiac structure covers a magnification range of around eight orders of magnitude, from the geometry of the cardiac chambers (Nielsen *et al*. 1991) down to descriptions of ion channel or T-tubule density and distribution (Soeller & Cannell 1999; Sommer & Jennings 1986). It is not yet practical to encompass complexity of this extent in an anatomical model of the heart. However, it should be possible to include detailed information about the geometry of the cardiac chambers (including the atria), the three-dimensional arrangement of cardiomyocytes and their associated extracellular matrix, the distribution and characteristics of the specialized cardiac conduction system and the architecture of the coronary circulation.

In this paper, we present an anatomically detailed finite-element model developed at the University of Auckland and adapted to include each of the aspects of cardiac morphology outlined above. In the Auckland heart model, tissue is assumed to be a continuum with orthotropic material properties based on comprehensive microstructural observations at points throughout the myocardium. Within the chapter, we also outline our current understanding of the anatomy and microstructure of the heart and indicate areas where more detailed information about cardiac structure is required.

2. The Auckland heart model

In this section, we provide an overview of the Auckland heart model. This is intended to serve as an introduction to the more detailed accounts given elsewhere (Hunter *et al*. 1993, 1997) and to define concepts and terms used in this article.

The Auckland heart model is based on a finite-element reference topology that matches the global geometry of the cardiac chambers. For example, the mesh shown in figure 1 represents right and left ventricles as an assembly of 24 three-dimensional elements.

Prolate spheroidal coordinates (λ, μ, θ) are used to define heart geometry in order to minimize the number of elements needed to represent the complex three-dimensional ventricular geometry. The reference prolate spheroidal coordinate system relates to rectangular Cartesian (x, y, z) and cylindrical polar (x, r, θ) coordinate systems as follows:

$$\left.\begin{aligned} x &= x = a\cosh\lambda\cos\mu, \\ y &= r\cos\theta = a\sinh\lambda\sin\mu\cos\theta, \\ z &= r\sin\theta = a\sinh\lambda\sin\mu\sin\theta, \end{aligned}\right\} \tag{2.1}$$

where a is the location of the focus of the prolate spheroidal coordinates on the x-axis. The λ coordinate is directed transmurally, the μ coordinate runs azimuthally from apex ($\mu = 0$) to base along an elliptical path, and the θ coordinate is circumferential with $\theta = 0$ placed at the centre of the right ventricular free wall. The x-axis forms the central base-to-apex axis of the heart and the y-axis passes through the centre of the right ventricular free wall.

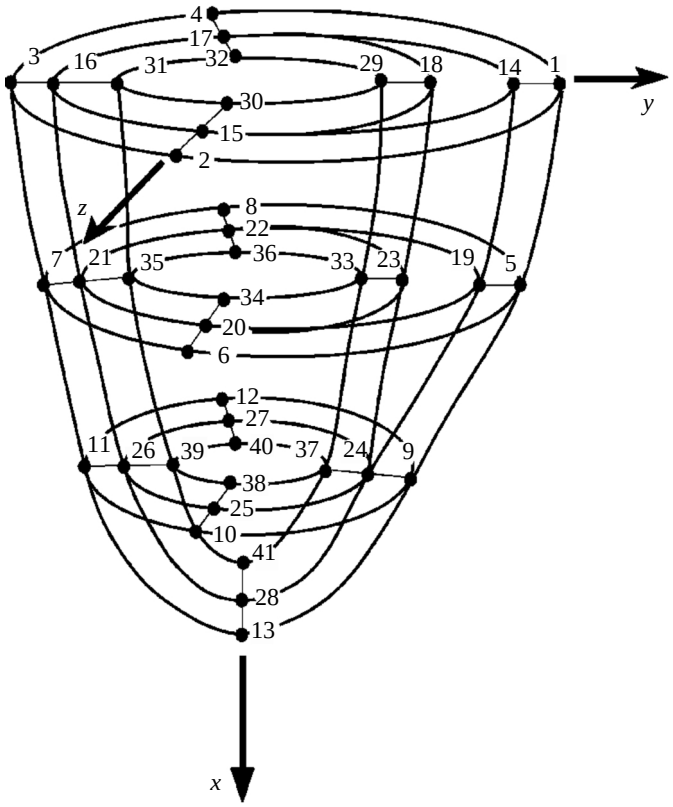

Figure 1. Schematic of finite-element mesh of left and right ventricles. Node numbers are shown. The free wall of the right ventricle is represented by four elements (nodes 1, 2, 4, 5, 6, 8, 9, 10, 12, 14, 15, 17, 19, 20, 22, 24, 25, 27). (From Nielsen *et al.* (1991).)

A material coordinate system is one which is attached to material particles and so moves with the material as it deforms. The material coordinates (ξ_1, ξ_2, ξ_3) are directly associated with element geometry, with ξ_1 in the circumferential direction, ξ_2 in the longitudinal (apex–base) direction, and ξ_3 in the transmural direction. A further material coordinate system, associated with the orthotropic structure of myocardium, is introduced later.

The spatial variation of structural information, such as surface geometry or myocyte orientation within each element, is approximated by linear polynomial interpolation of parameters defined at the element nodes. We make extensive use of linear Lagrange and cubic Hermite basis functions for this purpose.

The Lagrange basis functions $L_1(\xi) = 1-\xi$ and $L_2(\xi) = \xi$ produce a linear approximation of a scalar function within an element and ensure that continuity is maintained at element boundaries. For example, if ξ $(0 \leqslant \xi \leqslant 1)$ is a normalized measure of distance along a one-dimensional element, the function $u(\xi) = L_1(\xi)u_1 + L_2(\xi)u_2$ has the values u_1 and u_2 for $\xi = 0$ and $\xi = 1$, respectively (i.e. at the nodes). Therefore, linear Lagrange basis functions provide an efficient means of achieving piecewise linear interpolation between parameters defined at each finite-element node.

Similarly, we can use the trilinear Lagrange element basis to approximate a scalar function within a three-dimensional element:

$$\begin{aligned} u(\xi_1,\xi_2,\xi_3) = {} & L_1(\xi_1)L_1(\xi_2)L_1(\xi_3)u_1 + L_2(\xi_1)L_1(\xi_2)L_1(\xi_3)u_2 \\ & + L_1(\xi_1)L_2(\xi_2)L_1(\xi_3)u_3 + L_2(\xi_1)L_2(\xi_2)L_1(\xi_3)u_4 \\ & + L_1(\xi_1)L_1(\xi_2)L_2(\xi_3)u_5 + L_2(\xi_1)L_1(\xi_2)L_2(\xi_3)u_6 \\ & + L_1(\xi_1)L_2(\xi_2)L_2(\xi_3)u_7 + L_2(\xi_1)L_2(\xi_2)L_2(\xi_3)u_8. \end{aligned} \tag{2.2}$$

In this case there are eight nodal parameters, one at each corner of the three-dimensional element.

Linear Lagrange basis functions do not exhibit C^1 continuity: the spatial gradient of an interpolated function is not continuous across element boundaries. However, gradient continuity can be achieved using the one-dimensional cubic Hermite basis functions:

$$\left.\begin{aligned} H_1^0(\xi) &= 1 - 3\xi^2 + 2\xi^3, \\ H_1^1(\xi) &= \xi(\xi-1)^2, \\ H_2^0(\xi) &= \xi^2(3-2\xi), \\ H_2^1(\xi) &= \xi^2(\xi-1). \end{aligned}\right\} \tag{2.3}$$

With cubic Hermite basis functions it is possible to approximate complex spatial variation of a scalar function within an element. Specification of four parameters u, $\partial u/\partial\xi_1$, $\partial u/\partial\xi_2$ and $\partial^2 u/\partial\xi_1\partial\xi_2$ per node, allows two-dimensional interpolation of u with C^1 continuity across element boundaries. Tensor-product combinations of Lagrange and Hermite basis functions (e.g. bicubic Hermite in the (ξ_1,ξ_2)-plane and linear Lagrange in the ξ_3-direction, or bilinear Lagrange in the (ξ_1,ξ_2)-plane and cubic Hermite in the ξ_3-direction, etc.) can be used to provide a very flexible and powerful means of defining anatomical variables, such as the fibre and sheet angles, or dependent field variables, such as electrical potential or oxygen concentration, over the myocardium.

3. Geometry

In most previous studies, ventricular-cavity geometry has been reconstructed from serial transverse sections (Janicki *et al*. 1981; Lorange & Gulrajani 1993; Okajima *et al*. 1968). Typically, this has been carried out on fixed explanted hearts. However, using magnetic resonance imaging it is possible to reconstruct chamber geometry in the beating heart (Young *et al*. 1996). The advantages of such *in vivo* measurements are enormous, but there are limits on the resolution which can be achieved.

The geometry of the initial Auckland heart model was characterized by systematic mapping of three-dimensional points on epicardial and the endocardial surfaces of the right ventricle (RV) and the left ventricle (LV) of fixed dog hearts using a purpose-built cylindrical polar coordinate measurement rig (Nielsen *et al*. 1991). The spacing of the measurements was about 5 mm on the epicardial surface and about 2 mm on the endocardial surfaces. The resolution of the system was 0.1 mm.

The choice of prolate spheroid coordinates (λ,μ,θ) for geometric field variables provides a major advantage when fitting the nodal coordinates of the model to measured surface coordinates, because only the λ coordinate need be considered in the fitting process. The λ coordinate is approximated using a bicubic Hermite basis

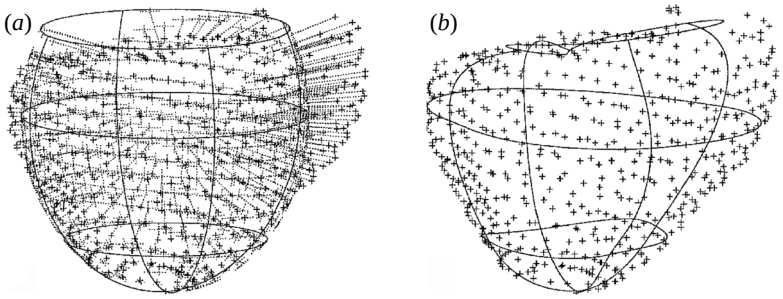

Figure 2. Least-squares fitting of finite-element nodal λ parameters to epicardial geometry measurements from a perfusion-fixed canine heart. Data points projected onto (*a*) initial prolate spheroid mesh and (*b*) optimized finite-element surface mesh. The dotted line projections are from data points to sites on the mesh with the same μ and θ coordinates. (From Nielsen *et al.* (1991).)

function in the (ξ_1, ξ_2)-plane and a linear basis function in the ξ_3-direction. This provides sufficient degrees of freedom to model the complex surface geometry of the heart chambers. Trilinear basis functions are used for the variables μ and θ.

Geometric fitting was carried out separately for the epicardial surface and the two cavity surfaces. Consider a data point d on the epicardial surface that is projected back onto the element surface along lines of constant μ and θ. $\lambda(\xi_1^d, \xi_2^d)$ is the λ coordinate of the projected point on the element surface and is obtained from a bicubic Hermite interpolation of element node parameters λ, $\partial\lambda/\partial\xi_1$, $\partial\lambda/\partial\xi_2$ and $\partial^2\lambda/\partial\xi_1\partial\xi_2$.

To estimate the best-fit combination of these nodal parameters, we minimize the sum of squares below over all data points:

$$S = \sum_{d=1}^{D} W_d(\lambda(\xi_1^d, \xi_2^d) - \lambda_d)^2, \tag{3.1}$$

where W_d is a weight associated with data point d.

Initial and final phases of this fitting process are presented in figure 2 for a typical epicardial surface dataset using the finite-element mesh illustrated in figure 1. Although minimizing equation (3.1) is not the same as minimizing a Euclidean norm, the difference in fitting surface parameters is negligible in comparison with mean measurement error and the computational cost of this linear fitting procedure is orders of magnitude less than the cost of the nonlinear procedure (Nielsen *et al.* 1991). An additional benefit of using prolate spheroidal coordinates is that a reasonable first-order (confocal ellipsoid) approximation to the LV may be obtained with one element only. A further advantage is that a, the prolate spheroidal focus parameter, provides a convenient means of scaling the overall size of a model heart, e.g. to compare the shapes of hearts of different weights.

The full geometric model is assembled by combining the nodal parameters for each of the surface fits. Because the nodal values of μ and θ coordinates and arc length-scale factors are fixed, there are four degrees of freedom per node in fitting parameters for surface geometry. For the finite-element topology in figure 1, there are 52 degrees of freedom for the epicardial and LV endocardial surfaces with 44 degrees of freedom for the RV endocardial surface. This model provides a faith-

ful representation of epicardial surface geometry with RMS fitting errors less than 0.9 mm in all cases. Fitted cavity geometry reproduces papillary muscles but cannot resolve endocardial trabeculae. The RMS errors for endocardial surfaces are typically of the order of 1.8–2.7 mm. The fitting procedures required less than 10 s on an SGI O2 computer. Data from a large number of dog hearts were fitted and compared after scaling for longitudinal dimension, revealing remarkable consistency in shape and wall thickness (Hunter *et al*. 1993). Finally, it should be noted that the use of prolate spheroidal coordinates to represent ventricular geometry also has some disadvantages. In particular, it imposes constraints on the goodness of fit towards the base of the ventricles.

At present, our heart model incorporates only the geometry of the ventricles. An appropriate finite-element topology for atrial chambers and veno-atrial junctions together with inlet and outlet valve rings has been defined. There is a pressing need to characterize the geometry of these structures, this will require a measurement system with more degrees of freedom than the rig used to map the ventricular epicardial and endocardial surfaces. Moreover, because of its complexity, it will be necessary to represent this geometry in Cartesian coordinates rather than cylindrical polar or prolate spheroidal coordinates.

4. Myocardial architecture

Many previous descriptions of cardiac architecture have been biased by the view that the organization of ventricular myocardium and skeletal muscle are similar and by the use of relatively crude blunt dissection techniques which reinforced that view. Thus, in the first half of the 20th century, the ventricles were seen to consist of discrete muscle bundles which inserted into the atrio-ventricular (AV) valve ring and followed a complex helicoidal pathway through the ventricular wall (Mall 1911; Robb & Robb 1942). More recently, the ventricular walls have been incorrectly described as being composed of strap-like muscles (Torrent-Guasp *et al*. 1997).

A very different conception emerged from work reported by Lev & Simkins (1956) and Streeter & Bassett (1966). Ventricular myocardium was described as a continuum in which myocyte orientation varied smoothly across the ventricular wall from subepicardium to subendocardium. This view has informed most computer models of the heart, which assume that ventricular myocytes are uniformly coupled to form a syncitium with material properties that are transversely isotropic with respect to the local muscle 'fibre' axis. However, there is substantial discontinuity in the muscular architecture of the ventricles at both microscopic and macroscopic levels (Feneis 1943; Hort 1957; Spotnitz *et al*. 1974; Weisman *et al*. 1988) and it is most appropriate to view ventricular myocardium as a three-dimensional hierarchy of interconnecting muscle layers.

Two techniques developed in our laboratory provide a clearer picture of the laminar hierarchy of ventricular myocardium. The first is the use of low-power scanning electron microscopy (SEM) to image ventricular specimens, carefully registered with respect to ventricular geometry and sectioned orthogonal to the local myocyte axis (LeGrice *et al*. 1995*a*). As shown in figure 3, myocytes are arranged in discrete layers, on average four cells thick, separated by cleavage planes and coupled via an extensive extracellular connective tissue network. There is also direct branching between layers with muscle bridges one to two cells thick.

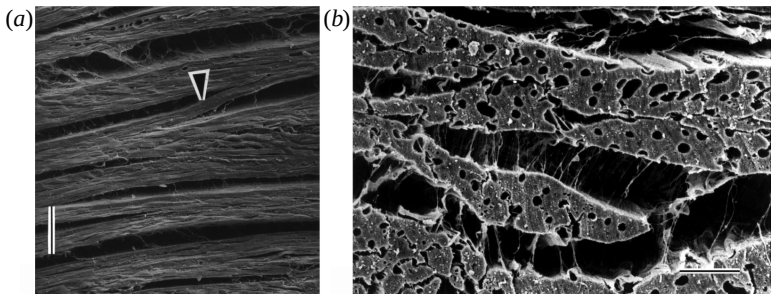

Figure 3. (*a*) SEM of ventricular myocardium sectioned parallel to epicardial surface. Scale bar 100 μm. Note the laminar arrangement of myocytes. Arrow shows muscle bridge between sheets. (*b*) SEM of ventricular myocardium sectioned transverse to myocyte axis. Scale bar 25 μm. Capillaries and perimysial collagen network are evident. (From LeGrice *et al.* (1995*a*).)

Figure 4. Oblique view of extended volume image from the LV of rat heart obtained using confocal microscopy. Note the laminar organization and collagen (white) interconnecting layers of myocytes. The epicardial collagen weave is clearly seen along with cleavage planes between myocardial layers. (From Young *et al.* (1998), with permission from the Royal Microscopical Society.)

More recently, we have developed a new technique to image extended volumes of myocardium (Young *et al.* 1998). These studies were carried out on resin-embedded transmural segments of rat ventricular myocardium. A contiguous set of z-series images covering the upper surface of the specimen was acquired using a confocal microscope: maximum imaging depth was 70 μm and spatial resolution was 1.5 μm. The upper surface of the specimen was then trimmed using a microtome and the process was repeated to assemble image volumes spanning up to 800 μm × 800 μm × 4.5 mm and typically consisting of 650 million voxels. Digital reslicing, segmentation and volume rendering methods can be applied to the resulting volumes to provide quantitative structural information about the three-dimensional organization of myocytes, extracellular collagen matrix and blood vessel network of the heart which has not previously been available.

On the basis of these and other observations we have developed the conceptual model of myocardial architecture shown in figure 6.

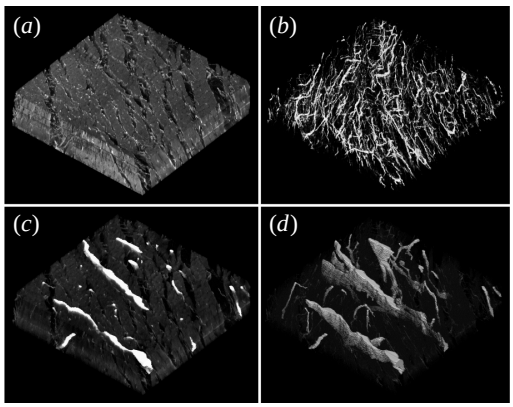

Figure 5. Reconstructed subvolumes. In the upper panel collagen is segmented and rendered (a) with and (b) without background due to myocytes. In the lower panel venous sinuses are segmented and rendered, (c) with, and (d) without background. (From Young *et al*. (1998), with permission from the Royal Microscopical Society.)

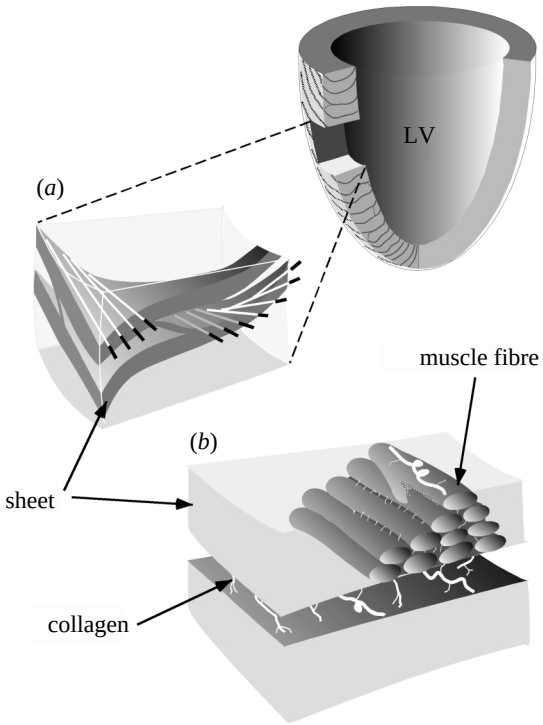

Figure 6. Schematic of cardiac microstructure. (a) A transmural block cut from the ventricular wall shows orientation of fibres. Note the transmural variation in fibre angle. (b) The muscle fibres are shown forming a layer three to four cells thick. Endomysial collagen is shown connecting adjacent cells within a sheet, while perimysial collagen links adjacent sheets. (Modified from LeGrice *et al*. (1995*a*).)

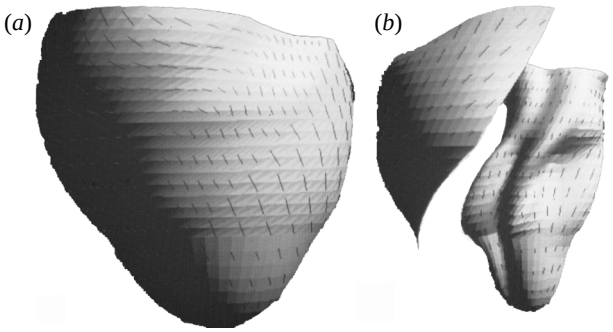

Figure 7. Anterior views of (*a*) epicardium and (*b*) endocardial surfaces of the RV and the LV. Fibre orientation vectors are projected onto these surfaces.

Groups of tightly coupled myocytes are arranged in layers which extend radially across the ventricular wall. The three-dimensional organization of layers and the extent of branching between them varies transmurally to accommodate local myocyte orientation.

It appears that the laminar architecture of ventricular myocardium has significant implications for electrical and mechanical function in normal and abnormal hearts (LeGrice *et al*. 1995*b*; Olivetti *et al*. 1990; Spotnitz *et al*. 1974; Weisman *et al*. 1988). In the Auckland model we therefore define a second set of material coordinates associated with this structure (LeGrice *et al*. 1997). One coordinate is in the direction of the myocyte axis, one transverse to this axis in the plane of the layers and the third orthogonal to the other two (perpendicular to the layers).

(*a*) *Myocyte orientation*

Detailed observations of ventricular myocyte orientation have been made in a range of species (Armour & Randall 1970; Fox & Hutchins 1972; Greenbaum *et al*. 1981; Jouk *et al*. 1995; McLean & Prothero 1987; Ross & Streeter 1975; Streeter & Bassett 1966). In general, standard histological techniques have been employed using myocardial samples from a limited number of representative ventricular sites. The work has extended to comparisons of fibre orientation during systole and diastole (Streeter *et al*. 1969) and in normal and pathological hearts (Carew & Covell 1979). These studies reveal that myofibre orientation changes relatively smoothly through up to 180° across the free wall or interventricular septum with myocytes oriented below the circumferential direction on the epicardial surface and near perpendicular at the endocardial surfaces of both ventricles (see figure 7).

We have made extensive measurements of ventricular myocyte orientation in a series of normal dog hearts using a technique which explicitly preserves the registration of fibre orientation with respect to ventricular geometry (Nielsen *et al*. 1991). The ventricular walls were progressively shaved away in 0.5 mm steps and fibre orientations were mapped out at points on the exposed surface, together with the three-dimensional coordinates of those points. For each heart, this resulted in approximately 10 000 data points describing the fibre orientation throughout right and left ventricles. Our results confirm previous findings and demonstrate surprising consistency at corresponding ventricular sites in different dog hearts. However, there is significant local variation of fibre orientation, particularly in the interventricular

septum and towards the boundaries of LV and RV free walls, and this information cannot be obtained from the restricted datasets published by previous workers.

To incorporate our data into the finite-element model, fibre angle (α) is approximated using linear basis functions in the ξ_1- and ξ_2-directions and a cubic Hermite basis function in the ξ_3- (transmural) direction. The nodal values of α and $\partial\alpha/\partial\xi_3$ are fitted to the experimental measurements using a refined mesh. Given the predictability of transmural fibre orientation at corresponding sites in hearts of the same species, it is appropriate to use a single dataset in a representative computer model.

Our data are obtained by sectioning the ventricular wall parallel to the epicardial tangent plane to reveal the myocardial layers. Fibre orientation is estimated by measuring the orientation of the myocardial layers in that plane on the assumption that the myocyte axis is parallel to the epicardial tangent plane. However, at some sites, such as the ventricular base, the myocyte axis has a significant transmural component, defined as the imbrication angle (Streeter 1979). While our heart model allows for the definition of this angle, there have been no extensive measurements of fibre imbrication in the ventricle to date. However, detailed information on myocyte imbrication can be obtained using three-dimensional reconstruction techniques such as the extended confocal imaging technique outlined above.

(*b*) *Muscle layers*

Observations on the transmural organization of muscle layers have been made on segments removed from different LV sites in fixed dog hearts. SEM images for a series of samples from these segments reveal consistent patterns in cellular organization of muscle layers. Layers are 4 ± 2 myocytes thick at all transmural sites. However, there is a consistent transmural variation in the number of branches between layers and the extent of cleavage planes between layers. Specifically, there are two to threefold fewer branches in the midwall than in subepicardium (or subendocardium), and the extent of cleavage planes is greatest in the midwall. These observations on the transmural variation of laminar architecture using SEM techniques were consistent for a series of different ventricular sites (LeGrice *et al*. 1995*a*) and have subsequently been confirmed using extended confocal microscopy (Young *et al*. 1998).

Muscle layer orientations have also been recorded systematically in thick longitudinal transverse sections from normal dog hearts (LeGrice *et al*. 1995*a*). The technique employed is consistent with the method used to quantify muscle fibre orientation, in that layer orientation is carefully registered with respect to ventricular geometry. A schematic of transverse layer organization is given in figure 8, showing that orientations are generally normal to the ventricular surfaces in the midwall with some regional differences in the pattern of transmural variation. This variation is similar at the equator for RV and LV free walls, with orientation progressively changing from about $-90°$ (from radial) at the endocardium to 30–60° at the epicardium. For the interventricular septum, however, the transmural variation is generally opposite in sense changing from $+90°$ in the LV endocardium to about $-90°$ in the RV subendocardium. These observations were consistent across a number of hearts. A further notable characteristic of the laminar organization is the regular appearance of small regions in which layers are perpendicular to the predominant direction. While not particularly extensive in canine myocardium, this intersecting pattern is marked in pig myocardium (I. LeGrice 1994, unpublished observation). The significance of this

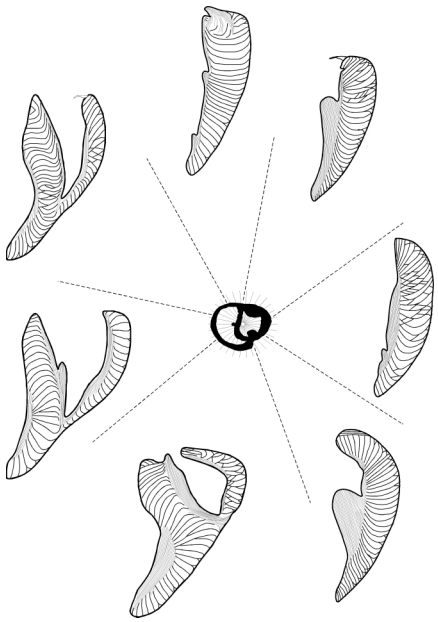

Figure 8. Apex–base transmural sections of the ventricles from a series of circumferential locations in a dog heart. The orientations of myocardial laminae are shown for each section (sketched from original data). (Modified from LeGrice *et al.* (1995*a*).)

variation is not yet known, though it is likely to be important for accommodating the significant shear deformation which occurs in myocardium throughout the cardiac cycle, the perpendicular cleavage planes aligning with the two orthogonal planes of maximum shear.

To incorporate transmural laminar organization into the finite-element model, layer orientation γ is approximated using linear basis functions in the ξ_1- and ξ_2-directions and a cubic Hermite basis function in the ξ_3- (transmural) direction. The nodal values of γ and $\partial\gamma/\partial\xi_3$ are fitted to the experimental measurements. When fitted within the finite-element model, the two sets of angles (α and γ) together yield a description of the three-dimensional laminar orientation throughout the heart. The methods described above mean that the fibre and layer orientation information used for the model are obtained separately from different hearts. Accurate characterization of local material coordinates therefore relies on the consistency of this structural information between hearts. Alternatively, transmural blocks can be removed from different sites in a single heart and measurements made from orthogonal planes (LeGrice *et al.* 1995*b*), but this can be done at only a limited number of sites.

(*c*) *Connective tissue*

The muscular architecture of ventricular myocardium is mirrored by the three-dimensional organization of the associated extracellular connective tissue matrix. The main components of the connective tissue hierarchy were initially described by Caulfield & Borg (1979) and Robinson *et al.* (1983) and include connective tissue surrounding and interconnecting myocytes (endomysium), and connective tissue surrounding and interconnecting bundles of muscles (perimysium). Other investigations

have focused on details such as morphology of coiled perimysial fibres (Robinson *et al.* 1988*b*), cardiac collagen types (Bashey *et al.* 1992; Robinson *et al.* 1988*a*), and changes in the cardiac extracellular connective tissue matrix with pathology (Janicki *et al.* 1981; Sato *et al.* 1983; Weber *et al.* 1994).

Recent studies carried out in our laboratory have enabled us to visualize the three-dimensional arrangement of the perimysial collagen network across the ventricular wall (LeGrice *et al.* 1995*a*; Young *et al.* 1998). This work reveals that the perimysial collagen network is densest in the subendocardium and subepicardium and relatively sparse in the midwall. On the other hand, the length and tortuosity of perimysial collagen cords connecting adjacent muscle layers was greatest in the midwall of the ventricles.

Comprehensive morphometric data on the three-dimensional organization of the connective tissue matrix throughout the ventricular wall are necessary in order to establish realistic material laws for ventricular myocardium (Smaill & Hunter 1991). Simple measurements of connective tissue volume as revealed by hydroxyproline assays or area fraction techniques cannot provide this information. Extended three-dimensional imaging methods such as the confocal microscope technique outlined above (see figure 5) are seen to provide a promising approach to this problem.

5. Specialized conduction system

There is a wealth of information available on the microstructure and electrical properties of the sinoatrial (SA) and atrio-ventricular (AV) nodes (Coppen *et al.* 1999; Racker & Kadish 2000). Similarly, the subendocardial distribution of the Purkinje fibre network, which determines the pattern of myocardial activation in sinus rhythm, has been comprehensively studied using a range of techniques (Durrer *et al.* 1970; Myerburg *et al.* 1975; Scher *et al.* 1953). While the proximal fast-conduction system has been well described, this is not the case for the intramural distribution of Purkinje fibres. There is evidence that the transmural extent of the fast-conduction network varies between species, with the system confined to the subendocardium in the human and rabbit (Ansari *et al.* 1999; Oosthoek *et al.* 1993; Tranum-Jensen *et al.* 1991), but found through to the subepicardium in other species such as pig and sheep (Ansari *et al.* 1999; Holland & Brooks 1976; Tranum-Jensen *et al.* 1991). Information on the proximal Purkinje system has been incorporated into the Auckland model and the subendocardial distribution of the peripheral Purkinje fibre network has been generated using a 'fractal-like' process. Effort is currently being focused on quantifying the anatomy and electrical properties of SA and AV nodes in a form which can be incorporated into the model. However, data on the transmural penetration of Purkinje fibre network are also required, since this may affect the breakthrough of an ectopic activation into the conduction system.

6. Coronary circulation

The topology of coronary blood vessels on the epicardial surface of the heart has been quantified by a number of groups, including our own (Young *et al.* 1989). There are also extensive morphometric data on the hierarchy of intramural coronary arteries in the pig heart (Kassab *et al.* 1993). While characterization of coronary postcapillary vessels has been somewhat less systematic, extensive transmural venous

sinuses have been described (Young *et al*. 1998) and it would appear that these may contribute significantly to the capacitance of the coronary circulation. At present, our understanding of the spatial relationship between coronary blood vessels and muscle layers is limited. For instance, it is not clear whether small arteries and arterioles that supply the capillaries within muscle layers run preferentially in the cleavage planes between layers. This information is necessary to model the effect of mechanical deformation on vascular resistance during ventricular systole. In the Auckland model, the distribution of intramural coronary vessels down to 100 μm diameter has been generated from measured epicardial topology using a 'fractal-like' process constrained by structural rules derived from the Kassab data (Smith *et al*. 2000). The model does not currently include a description of the extensive cardiac lymphatic system or blood vessels less than 100 μm in diameter, though these will need to be incorporated so that assumptions of incompressibility can be based on an appropriate footing.

(*a*) *Future perspectives*

The Auckland heart model provides a detailed and realistic representation of important aspects of ventricular anatomy and it has been used by a number of research groups for integrative studies of cardiac electrical and mechanical function. The model is based on an extensive anatomic dataset collected systematically by ourselves and others over more than a decade. However, there is a need for comprehensive extension of this morphometric database in order to exploit the full potential of computer modelling. In particular, we require quantitative information on

(i) the geometry and muscular architecture of the atrial chambers,

(ii) the distribution and characteristics of the specialized conduction system, including the SA and AV nodes and the transmural penetration of Purkinje fibres, and

(iii) the architecture of the coronary circulation within the myocardium.

This information is required for the human heart and for the species most commonly used as animal models of cardiac disease. The database must include information on normal and pathological hearts at different developmental stages. This is an ambitious goal and will be achieved only with the development of appropriate high throughput systems for morphometric analysis.

References

Ansari, A., Ho, S. Y. & Anderson, R. A. 1999 Distribution of the Purkinje fibres in the sheep heart. *Anat. Rec.* **254**, 92–97.

Armour, J. A. & Randall, W. C. 1970 Structural basis for cardiac function. *Am. J. Physiol.* **218**, 1517–1523.

Bashey, R. I., Martinez-Hernandez, A. & Jimenez, S. A. 1992 Isolation, characterization, and localization of cardiac collagen type VI: associations with other extracellular matrix components. *Circ. Res.* **70**, 1006–1017.

Carew, T. E. & Covell, J. W. 1979 Fiber orientation in hypertrophied canine left ventricle. *Am. J. Physiol.* **263**, H487–H493.

Caulfield, J. B. & Borg, T. K. 1979 The collagen network of the heart. *Lab. Invest.* **40**, 364–372.

Coppen, S. R., Kodama, I., Boyett, M. R., Dobrzynski, H., Takagishi, Y., Honjo, H., Yeh, H. & Severs, N. J. 1999 Connexin45, a major connexin of the rabbit sinoatrial node, is co-expressed with connexin43 in a restricted zone at the nodal–crista terminalis border. *J. Histochem. Cytochem.* **47**, 907–918.

Durrer, D., van Dam, R. T., Freud, G. E., Janse, M. J., Meijler, F. L. & Arzbaecher, R. C. 1970 Total excitation of the isolated human heart. *Circulation* **41**, 899–912.

Feneis, H. 1943 Das Gefüge des Herzmuskels bei Systole und Diastole. *Morph. Jahrb.* **89**, 371–406.

Fox, C. C. & Hutchins, G. M. 1972 The architecture of the human ventricular myocardium. *Hopkins. Med. J.* **130**, 289–299.

Greenbaum, R. A., Siew, Y. H., Gibson, D. G., Becker, A. E. & Anderson, R. H. 1981 Left ventricular fibre architecture in man. *Br. Heart J.* **45**, 248–263.

Holland, R. P. & Brooks, H. 1976 The QRS complex during myocardial ischemia. An experimental analysis in the porcine heart. *J. Clin. Invest.* **57**, 541–550.

Hort, W. 1957 Untersuchungen uber die Muskelfaserdehnung und das Gefüge des Myokards in der rechten Herzkammerwand des Meerschweinchens. *Virchows Arch.* **329**, 649–731.

Hunter, P. J., Nielsen, P. M. F., Smaill, B. H., LeGrice, I. J. & Hunter, I. W. 1993 An anatomical heart model with applications to myocardial activation and ventricular mechanics. In *High-performance computing in biomedical research* (ed. T. C. Pilkington, B. Loftis, J. F. Thompson, S. L.-Y. Woo, T. C. Palmer & T. F. Budinger), ch. 1, pp. 3–26. CRC Press.

Hunter, P. J., Smaill, B. H., Nielsen, P. M. F. & LeGrice, I. J. 1997 A mathematical model of cardiac anatomy. In *Computational biology of the heart* (ed. A. V. Panfilov & A. V. Holden), pp. 171–215. Wiley.

Janicki, J. S., Weber, K. T., Gochman, R. F., Shroff, S. & Geheb, F. J. 1981 Three-dimensional myocardial and ventricular shape: a surface representation. *Am. J. Physiol.* **241**, H1–H11.

Jouk, P.-S., Usson, Y., Michalowicz, G. & Parazza, F. 1995 Mapping of the orientation of myocardial cells by means of polarized light and confocal scanning laser microscopy. *Microsc. Res. Tech.* **30**, 480–490.

Kassab, G. S., Rider, C. A., Tang, N. J. & Fung, Y. B. 1993 Morphometry of pig coronary arterial trees. *Am. J. Physiol.* **265**, H350–H365.

LeGrice, I. J., Smaill, B. H., Chai, L. Z., Edgar, S. G., Gavin, J. B. & Hunter, P. J. 1995*a* Laminar structure of the heart: ventricular myocyte arrangement and connective tissue architecture in the dog. *Am. J. Physiol.* **269**, H571–H582.

LeGrice, I. J., Takayama, Y. & Covell, J. W. 1995*b* Transverse shear along myocardial cleavage planes provides a mechanism for normal systolic wall thickening. *Circ. Res.* **77**, 182–193.

LeGrice, I. J., Hunter, P. J. & Smaill, B. H. 1997 Laminar structure of the heart: a mathematical model. *Am. J. Physiol.* **272**, H2466–H2476.

Lev, M. & Simkins, C. S. 1956 Architecture of the human ventricular myocadium. Technic for study using a modification of the Mall–MacCallum method. *Lab. Invest.* **5**, 396–409.

Lorange, M. & Gulrajani, R. M. 1993 A computer heart model incorporating anisotropic propagation. I. Model construction and simulation of normal activation. *J. Electrocardiol.* **26**, 245–261.

McLean, M. R. & Prothero, J. 1987 Coordinated three-dimensional reconstruction from serial sections at macroscopic and microscopic levels of resolution: the human heart. *Anat. Rec.* **219**, 434–439.

Mall, F. P. 1911 On the muscular architecture of the ventricles of the human heart. *Am. J. Anat.* **11**, 211–266.

Myerburg, R. J., Nilsson, K., Castellanos, A., Lazzara, R., Befeler, B. & Gelband, H. 1975 The intraventricular conducting system and patterns of endocardial excitation. *Adv. Cardiol.* **14**, 2–14.

Nielsen, P. M. F., LeGrice, I. J., Smaill, B. H. & Hunter, P. J. 1991 Mathematical model of geometry and fibrous structure of the heart. *Am. J. Physiol.* **260**, H1365–H1378.

Okajima, M., Fujino, T., Kobayashi, T. & Yamada, K. 1968 Computer simulation of the propagation process in excitation of the ventricles. *Circ. Res.* **23**, 203–211.

Olivetti, G., Capasso, J. M., Sonnenblick, E. H. & Anversa, P. 1990 Side-to-side slippage of myocytes participates in ventricular wall remodeling acutely after myocardial infarction in rats. *Circ. Res.* **67**, 23–34.

Oosthoek, P. W., Virágh, S., Lamers, W. H. & Moorman, A. F. M. 1993 Immunohistochemical delineation of the conduction system. II. The atrioventricular node and Purkinje fibres. *Circ. Res.* **73**, 482–491.

Racker, D. K. & Kadish, A. H. 2000 Proximal atrioventricular bundle, atrioventricular node, and distal atrioventricular bundle are distinct anatomic structures with unique histological characteristics and innnervation. *Circulation* **101**, 1049–1059.

Robb, J. S. & Robb, R. C. 1942 The normal heart. Anatomy and physiology of the structural units. *Am. Heart J.* **23**, 455–467.

Robinson, T. F., Cohen-Gould, L. & Factor, S. M. 1983 Skeletal framework of mammalian heart muscle. *Lab. Invest.* **49**, 482–498.

Robinson, T. F., Cohen-Gould, L., Factor, S. M., Eghbali, M. & Blumenfeld, O. O. 1988*a* Structure and function of connective tissue in cardiac muscle: collagen types I and III in endomysial struts and pericellular fibres. *Scanning Microsc.* **2**, 1005–1015.

Robinson, T. F., Geraci, M. A., Sonnenblick, E. H. & Factor, S. M. 1988*b* Coiled perimysial fibers of papillary muscle in rat heart: morphology, distribution, and changes in configuration. *Circ. Res.* **63**, 577–592.

Ross, M. A. & Streeter, D. D. J. 1975 Nonuniform subendocardial fiber orientation in the normal macaque left ventricle. *Eur. J. Cardiol.* **3**, 229–247.

Sato, S., Ashraf, M., Millard, R. W., Fujiwara, H. & Schwartz, A. 1983 Connective tissue changes in early ischemia of porcine myocardium: an ultrastructural study. *J. Molec. Cell. Cardiol.* **15**, 261–275.

Scher, A. M., Young, A. C., Malmgren, A. L. & Paton, R. R. 1953 Spread of electrical activity through the wall of the ventricle. *Circ. Res.* **1**, 539–547.

Smaill, B. & Hunter, P. 1991 Structure and function of the diastolic heart: material properties of passive myocardium. In *Theory of heart: biomechanics, biophysics, and nonlinear dynamics of cardiac function* (ed. L. Glass, P. Hunter & A. McCulloch), pp. 1–29. Springer.

Smith, N. P., Pullan, A. J. & Hunter, P. J. 2000 Generation of an anatomically based geometric coronary model. *Ann. Biomed. Engng* **28**, 14–25.

Soeller, C. & Cannell, M. B. 1999 Examination of the transverse tubular system in living cardiac rat myocytes by 2-photon microscopy and digital image-processing techniques. *Circ. Res.* **84**, 266–275.

Sommer, J. R. & Jennings, R. B. 1986 Ultrastructure of cardiac muscle. In *The heart and cardiovascular system* (ed. H. A. Fozzard, R. B. Jennings, A. M. Katz & H. E. Morgan), pp. 61–100. Raven Press.

Spotnitz, H. M., Spotnitz, W. D., Cottrell, T. S., Spiro, D. & Sonnenblick, E. H. 1974 Cellular basis for volume related wall thickness changes in the rat left ventricle. *J. Molec. Cell. Cardiol.* **6**, 317–331.

Streeter, D. D. J. 1979 Gross morphology and fiber geometry of the heart. In *Handbook of physiology* (ed. R. M. Berne, N. Sperelakis & S. R. Geigert), pp. 61–112. American Physiologiocal Society.

Streeter, D. D. J. & Bassett, D. L. 1966 An engineering analysis of myocardial fiber orientation in pig's left ventricle in systole. *Anat. Rec.* **155**, 503–511.

Streeter, D. D. J., Spotnitz, H. M., Patel, D. P., Ross, J. J. & Sonnenblick, E. H. 1969 Fiber orientation in the canine left ventricle during diastole and systole. *Circ. Res.* **24**, 339–347.

Torrent-Guasp, F. F., Whimster, W. F. & Redmann, K. 1997 A silicone rubber mould of the heart. *Technol. Health Care* **5**, 13–20.

Tranum-Jensen, J., Wilde, A. A. M., Vermeulen, J. T. & Janse, M. J. 1991 Morphology of electrophysiologically identified junctions between Purkinje fibers and ventricular muscle in rabbit and pig hearts. *Circ. Res.* **69**, 429–437.

Weber, K. T., Sun, Y., Tyagi, S. C. & Cleutjens, J. P. M. 1994 Collagen network of the myocardium: function, structural remodelling and regulatory mechanisms. *J. Molec. Cell. Cardiol.* **26**, 279–292.

Weisman, H. F., Bush, D. E., Mannisi, J. A., Weisfeldt, M. L. & Healy, B. 1988 Cellular mechanisms of myocardial infarct expansion. *Circulation* **78**, 186–201.

Young, A. A., Hunter, P. J. & Smaill, B. H. 1989 Epicardial surface estimation from coronary angiograms. *Comp. Vision Graphics Image Process.* **47**, 111–127.

Young, A. A., Orr, R., Smaill, B. H. & Dell'Italia, L. J. 1996 Three dimensional changes in left and right ventricular geometry in chronic mitral regurgitation. *Am. J. Physiol.* **271**, H2689–H2700.

Young, A. A., LeGrice, I. J., Young, M. A. & Smaill, B. H. 1998 Extended confocal microscopy of myocardial laminae and collagen network. *J. Microsc.* **192**, 139–150.